

Water, Methane, and Carbon Dioxide Present in the Dayside Spectrum of the Exoplanet HD 209458b

M. R. Swain¹, G. Tinetti², G. Vasisht¹, P. Deroo¹, C. Griffith³, J. Bouwman⁴, Pin Chen¹,
Y. Yung⁵, A. Burrows⁶, L. R. Brown¹, J. Matthews⁷, J. F. Roe⁹, R. Kuschnig⁸, & D.
Angerhausen¹⁰

ABSTRACT

Using the NICMOS instrument on the Hubble Space Telescope, we have measured the dayside spectrum of HD 209458b between 1.5–2.5 μm . The emergent spectrum is dominated by features due to the presence of methane (CH_4) and water vapor (H_2O), with smaller contributions from carbon dioxide (CO_2). Combining this near-infrared spectrum with existing mid-infrared measurements shows the existence of a temperature inversion and confirms the interpretation of previous photometry measurements. We find a family of plausible solutions for the molecular abundance and detailed temperature profile. Observationally resolving the ambiguity between abundance and temperature requires either (1) improved wavelength coverage or spectral resolution of the dayside emission spectrum, or (2) a transmission spectrum where abundance determinations are less sensitive to the temperature structure.

¹Jet Propulsion Laboratory, California Institute of Technology, 4800 Oak Grove Drive, Pasadena, CA 91109

²University College London, Gower Street, London WC1E 6BT, UK

³University of Arizona, Lunar and Planetary Laboratory, Space Science Bldg. Room 525, 1629 E. University Blvd. Tucson, AZ 85721

⁴Max-Planck Institute for Astronomy, Konigstuhl 17, D-69117 Heidelberg, Germany

⁵Division of Geological and Planetary Sciences, California Institute of Technology, Pasadena, CA 91125

⁶Dept. of Astrophysical Sciences, Princeton University, Princeton, NJ 08544

⁷Dept. of Physics & Astronomy, University of British Columbia, Vancouver, BC V6T 171 Canada

⁸NASA Ames Research Center, MS 244-30, Moffett Field, CA 94035

⁹Institut fur Astronomie, Universitat Wien Turkenschanzstrasse 17, A-1180 Wien, Austria

¹⁰Institute of Space Systems, University Stuttgart; DAAD-Fellow

Subject headings: planetary systems — techniques: spectroscopy

1. Introduction

HD 209458b has the distinction of being the first identified transiting extrasolar planet (Charbonneau et al. 2000). This 0.69 Jupiter-mass planet orbits a G0V stellar primary ($K_{mag}=6.3$) every 3.52 days and was the first exoplanet with a detected atmosphere (Charbonneau et al. 2002). It was also one of the first planets found to emit detectable amounts of infrared radiation (Deming et al. 2005). The dayside mid-infrared spectrum for this planet, based on Spitzer IRS observations, has been previously obtained (Richardson et al. 2007; Swain et al. 2008a). Mid-infrared dayside photometry (Knutson et al. 2008) provides evidence for an atmospheric temperature inversion (Burrows, et al. 2007) and has been used to support a classification scheme for the hot-Jupiter type exoplanets (Fortney et al. 2008). Mid-infrared photometric measurements of the orbital phase light curve of HD 209458b (Cowan, et al. 2007) find that the dayside and nightside brightness temperatures are similar. Models of atmospheric circulation for HD 209458b suggest that the zonal wind structure is a function of altitude (Showman et al. 2008), and mid-infrared dayside emission could vary (Rauscher et al. 2007, 2008; Showman et al. 2008).

The recent announcement of the detection of H_2O and CH_4 in the terminator regions of the hot-Jupiter HD 189733b (Swain, Vasisht & Tinetti 2008b; hereafter SVT08) via near-infrared spectroscopy using the Hubble Space Telescope (HST) demonstrated that molecular spectroscopy of bright transiting planets is possible. The subsequent HST detection of H_2O , CO_2 , and carbon monoxide (CO) on the dayside of HD 189733b provides significant constraints for atmospheric models and suggests that exoplanet molecular spectroscopy may become routine (Swain et al. 2009; hereafter S09) in the near future. This is significant because molecules provide a powerful tool for determining the conditions, composition, and chemistry of exoplanet atmospheres. In this paper, we report on the first ever spectroscopic detection of molecules in the atmosphere of HD 209458b, making this the second exoplanet for which molecular spectroscopy has now been demonstrated.

2. Observations & Data Analysis

We observed HD 209458 for five consecutive HST orbits using the NICMOS camera in imaging-spectroscopy mode covering the wavelengths 1.5–2.5 μm using the G206 grism. As in previous observations (SVT08, S09), the DEFOCUS mode was used, resulting in a

spectral resolution of $R \simeq 40$. Observations were conducted on June 15, 2008, from UT 09:38:59 to UT 16:45:24. A total of 310 usable snapshot spectra were acquired with an individual exposure time of $T = 4.06$ s. Using the system ephemeris (Knutson et al. 2007) we determine that the bulk of the first two orbits (O_1 & O_2) coincides with the pre-ingress light curve, the third and part of the fourth orbit (O_3 & O_4) cover the occultation, while the fifth orbit (O_5) is post-egress (see Fig. 1). We find that 75 exposures cover the full eclipse, 43 exposures are in ingress/egress, and 192 exposures cover the pre-ingress or post-egress intervals. The effective exposure time for each spectrum was $T = 4.06$ s. To determine the spectrometer wavelength calibration, narrow band (F190) filter calibration exposures were acquired during O_1 .

Our data analysis methods, based on decorrelation of instrument parameters from the measured spectrophotometric light curves, have been described previously (SVT08, S09). For the results presented here, the data-analysis approach remains largely unchanged but is updated in two significant ways. First, the decorrelation for instrument parameters is based on detector pixel values; in the past we averaged the detector data to the defocused spectral resolution prior to the decorrelation. The new approach has the advantage of determining the corrected, decorrelated spectrum using the full oversampling of the instrument. Second, we now derotate and shift the spectrum (via interpolation) to achieve the same sampling at all wavelengths and times. This effectively places observations in a common, pixel-based, reference frame. We tested this new reduction method by computing a dayside spectrum of HD 189733b and comparing it to our previous result (S09); the agreement between the two methods was found to be excellent, with differences between the spectra always within the statistical uncertainty of the measurement. As with our previous observations of the primary and secondary eclipse of HD 189733b, we found the instrument parameters for the first orbit, O_1 , differed significantly from the remaining orbits, O_2 – O_5 ; following our previous approach (SVT08, S09), we omitted the O_1 spectra from the analysis. To add an additional constraint to any possible orbit-to-orbit brightness changes, we arranged for contemporaneous, high-precision, visible photometry using the Micro-variability and Oscillations of Stars (MOST) satellite (Walker et al. 2003). The MOST observations were timed to provide a photometry measurement during each HST orbit (see Fig. 1), and the data were calibrated using the method described by Rowe et al. (2008).

3. Discussion

The near-infrared dayside spectrum of HD 209458b shows three clear peaks at 1.6, 1.8–1.9, and 2.2 μm , while between the peaks the flux density decreases to near-zero (within the

measurement error). The spectrum has an average uncertainty per data point of $\sim 7.5 \times 10^{-5}$, corresponding to a dynamic range of 13,300:1 (75 ppm), with a wavelength resolution of $\frac{\lambda}{\Delta\lambda} = 35$ at $2 \mu\text{m}$. To maximize wavelength coverage for the spectral interpretation, we incorporated mid-infrared Spitzer photometry data (Knutson et al. 2008) and spectroscopy data (originally obtained by Richardson et al. 2007). We have previously undertaken our own calibration of these Spitzer IRS data (Swain et al. 2008a), and we use those results in the discussion that follows.

The interpretation of the data was done using two independent spectral retrieval methods incorporating a line-by-line radiative transfer model (Griffith, et al. (1998); Tinetti et al. (2007a,b), SVT08, S09), and the results from both models are in agreement. The radiative transfer calculations assume local thermal equilibrium (LTE) conditions, as expected for pressures exceeding 10^{-3} bar that are probed by the near-infrared spectrum. We evaluated a variety of temperature (T) together with the effects of CH_4 , H_2O and CO_2 , which are assumed to have constant mixing ratios. We use the CH_4 line list of Nassar & Bernath (2003) for temperatures at 800, 1000, and 1273 K to quantify the affects of CH_4 at wavelengths of 1.58–2.5 μm , outside of which we use absorption parameters by Rotham et al. (2005). The hot water lines from Barber et al. (2006) and Zobov et al. (2008) were used to quantify the water features. Absorption by CO_2 is calculated from the HITRAN hot CO_2 line list (Tashkun et al. 2003). Absorption coefficients of H_2O and CO_2 are calculated using line-by-line techniques every 0.004 cm^{-1} wavenumbers. The radiative transfer calculation has 80 vertical grid points that extend from 10^{-7} to 10 bar. The effects of particulates are excluded.

The combination of near-infrared and mid-infrared data probes the temperature profile over a pressure range of a few bars to 10^{-5} bars and provides evidence for a temperature inversion. The 8 μm brightness temperature is 1770 K, while the 2.2–2.4 μm brightness temperature ranges from 1100–1600 K; this temperature difference, combined with the difference in pressure probed by these wavelengths, indicates the presence of a temperature inversion. We find that a temperature inversion could occur somewhere between $\sim 10^{-1}$ – 10^{-4} bar, where temperatures increase by roughly 500–700 K. This temperature-inverted region resembles those of planetary stratospheres; it occurs at a similar pressure level and causes a convectively stable temperature profile. The model spectrum from three exemplar temperature profiles (inverted) are shown in Fig. 3 (together with a temperature profile with no inversion), and the model residuals (Fig. 4) show the improved fit with a temperature inversion. The presence of the stratosphere coupled with a relatively steep stratospheric temperature gradient implies the existence of a local absorber that heats the atmosphere and maintains the local temperature structure. The temperature profile we derive confirms the previous identification of a T inversion (Burrows, et al. 2007; Knutson et al. 2008), but

the profile reported here differs in terms of the detailed shape.

Our estimates for the temperature profile and molecular mixing ratios are based on modeling the combined near-infrared and mid-infrared data sets. However, the recent finding of variability in the mid-infrared emission spectrum of HD 189733b (Grillmair et al. 2008) suggests caution is needed when deriving constraints from the noncontemporaneous mid-IR data. Although the presence of H₂O and CH₄ can explain most of the spectrum, we find that an additional absorber is required around 2.1 μm , and we attribute this to CO₂. The evidence for a temperature inversion comes from the mid-infrared spectrum, and the mid-infrared data provide some additional constraints on the mixing ratios for H₂O and CO₂. We find that a range of temperature profiles and molecular mixing ratios are consistent with the data as illustrated by the models shown in Fig. 4 and the sample contribution functions shown in Fig. 5, which correspond to three possible temperature profiles. Providing improved observational constraints on the location of the tropopause and the molecular mixing ratios will require additional observations, for which there are two possibilities. The first is to improve the spectral coverage and/or spectral resolution of the dayside spectrum, which could be done in the future with JWST. The second is to use a transmission spectrum (obtained during primary eclipse) to estimate the molecular abundances in the terminator regions; subject to some assumptions, this could be used to place constraints on the abundance of one or more molecules. HST transmission spectra for this planet have been obtained and are being analyzed by our team. However, the interpretation of the transmission spectrum is complex due to the presence of temporal variability (the subject of a forthcoming paper).

There are two important caveats concerning our derived temperature profiles. First is the assumption of emission from a uniform disk rather than from a realistic irradiated hemisphere; as such, the spectrum and T-profile we derive is disk-averaged. Second, the spectral retrieval process used in our best fitting models implicitly acknowledges the possible role of dynamics in establishing atmospheric temperature by relaxing typical 1-line model constraints on the temperature gradient. Thus, portions of the atmosphere of HD 209458b may support departures from radiative equilibrium. Fully self-consistent modeling would require handling heat advection in the context of a global circulation model, which is beyond the scope of this paper. It is worth noting that the presence of a relatively strong dayside temperature inversion significantly complicates the spectral retrieval process for HD 209458b relative to the case of HD 189733b.

Given that the dayside emission spectra for HD 189733b and HD 209458b have been observed with nearly identical instrument configurations, we can make a preliminary comparison of these two planets (see Fig. 6). For the present, we restrict this discussion to the near-infrared to avoid the complications introduced by the presence of mid-infrared vari-

ability observed in HD 189733b (Grillmair et al. 2008). In both planets, the near-infrared dayside emission spectrum probes the $5 \leq P \leq 10^{-2}$ bar portion of the atmosphere. Similarities – both planets show the presence of H₂O, CO₂, and $\frac{dT}{dP} \leq 0$ for pressures near 1 bar. Differences – the abundance of CH₄ is significantly enhanced in HD 209458b relative to HD 189733b, and the temperature at 1 bar is higher in HD 209458b, as well. The observed differences in the near-infrared dayside spectra of these two hot-Jupiters are likely due to differences in temperature and composition; HD209458b is dominated by CH₄ absorption features, while HD 189733b is dominated by absorption from H₂O and CO₂.

4. Conclusions

In summary, we have presented the first near-infrared spectrum of light emitted by HD 209458b. Using an iterative forward model approach for spectral retrieval, we find that H₂O, CH₄, and CO₂, together with a temperature inversion, are present in the dayside atmosphere of HD 209458b. There are a range of temperature profiles and molecular abundance solutions that are consistent with the data. Additional observational constraints on the atmospheric temperature structure and composition will require either improved wavelength coverage/spectral resolution for the dayside spectrum or a transmission spectrum. We note that some of the temperature profiles consistent for these observations raise the question of whether the dayside atmosphere is in radiative equilibrium. Although advection of heat could support departures from radiative equilibrium, our present knowledge of most molecular opacities at high temperatures limits our ability to determine decisively whether the radiative equilibrium condition is met or not; thus there is an urgent need for further laboratory studies to obtain molecular databases for determining high temperature opacities of the most common molecules expected in hot-Jupiter atmospheres.

We appreciate the Director’s time award for these observations, and we thank Tommy Wiklind, Beth Padillo, and other members of the Space Telescope Science Institute staff for assistance in planning the observations. We also thank Jonathan Tennyson and Bob Barber for help with the water line list. G. Tinetti was supported by the Royal Society. A portion of the research described in this paper was carried out at the Jet Propulsion Laboratory, under a contact with the National Aeronautics and Space Administration.

REFERENCES

Barber, R. J., Tennyson, J., Harris, G. J. & Tolche nov, R. N. 2006, MNRAS, 368, 1087

- Burrows, A., Hubeny, I, Budaj, J., Knutson, H. A. & Charbonneau, D. 2007, ApJ, 668, 171
- Charbonneau, D., Brown, T. M., Latham, D. W., & Mayor, M. 2000, ApJ, 529, 45
- Charbonneau, D., Brown, T. M., Noyes, R. W., & Gilliland, R. L. 2002, ApJ, 568, 377
- Cowan N. B., Agol, E., & Charbonneau, D. 2007, MNRAS, 379, 641
- Deming, D., Seager, S., Richardson, L. J., & Harrington, J. 2005, Nature, 434, 740
- Fortney, J. J., Marley, M. S., Saumon, D., & Lodders, K. 2008, ApJ, 683, 1104
- Griffith, C. A., Yelle, R. V. & Marley, M. S. 1998, Science, 282, 2063
- Grillmair, C. J, Burrows, A., Charbonneau, D., Armus, L, Stauffer, J., Meadows, V., Van
Cleve, J., von Braun, K., & Levine, D. 2008, Nature, 456, 767
- Knutson, H. A., Charbonneau, D., Noyes, R. W., Brown, T. M., & Gilliland, R. L. 2007,
ApJ, 655, 564
- Knutson, H. A., Charbonneau, D., Allen, L. E., Burrows, A., & Thomas, M. S. 2008, ApJ,
673, 526
- Nassar, R., & Bernath, P. 2003, JQRST, 82, 279
- Rauscher, E. et al. 2007, ApJ, 664, 1199
- Rauscher, E., Kristen, M., Cho, J. Y.-K, Seager, S., Hansen, B. M.S. 2008, ApJ, 681, 1646
- Rotham, L. S. et al. 2005, JQSRT, 92, 139
- Rowe, J. F. 2008, arXiv:0711.4111v2
- Richardson, J. L., Deming, D., Horning, K, Seager, S., & Harrington, J. 2007, Nature, 445,
892
- Showman, A. P., Cooper, C. S., Fortney, J. J., & Marley, M. S. 2008, ApJ, 682, 559S
- Swain, M. R., Bouwman, J., Akeson, R. L., Lawler, S., & Beichman, C. A. 2008a, ApJ, 674,
482
- Swain, M. R., Vasisth, G. V., & Tinetti, G. 2008b, Nature, 452, 329
- Swain M. R. et al. 2009, ApJ, 960, L114

Tashkun, S. A., Perevalov, V. I., Tefflo, J-L., Bykov, A. D., Lavrentieva, N. N. 2003, JQSRT, 82, 165

Tinetti, G. et al. 2007a, ApJ, L99

Tinetti, G. et al. 2007b, Nature, 448, 169

Walker, G. et al. 2003, PASP, 115, 1023

Zobov, N. F. et al. 2008, MNRAS, 387, 1093

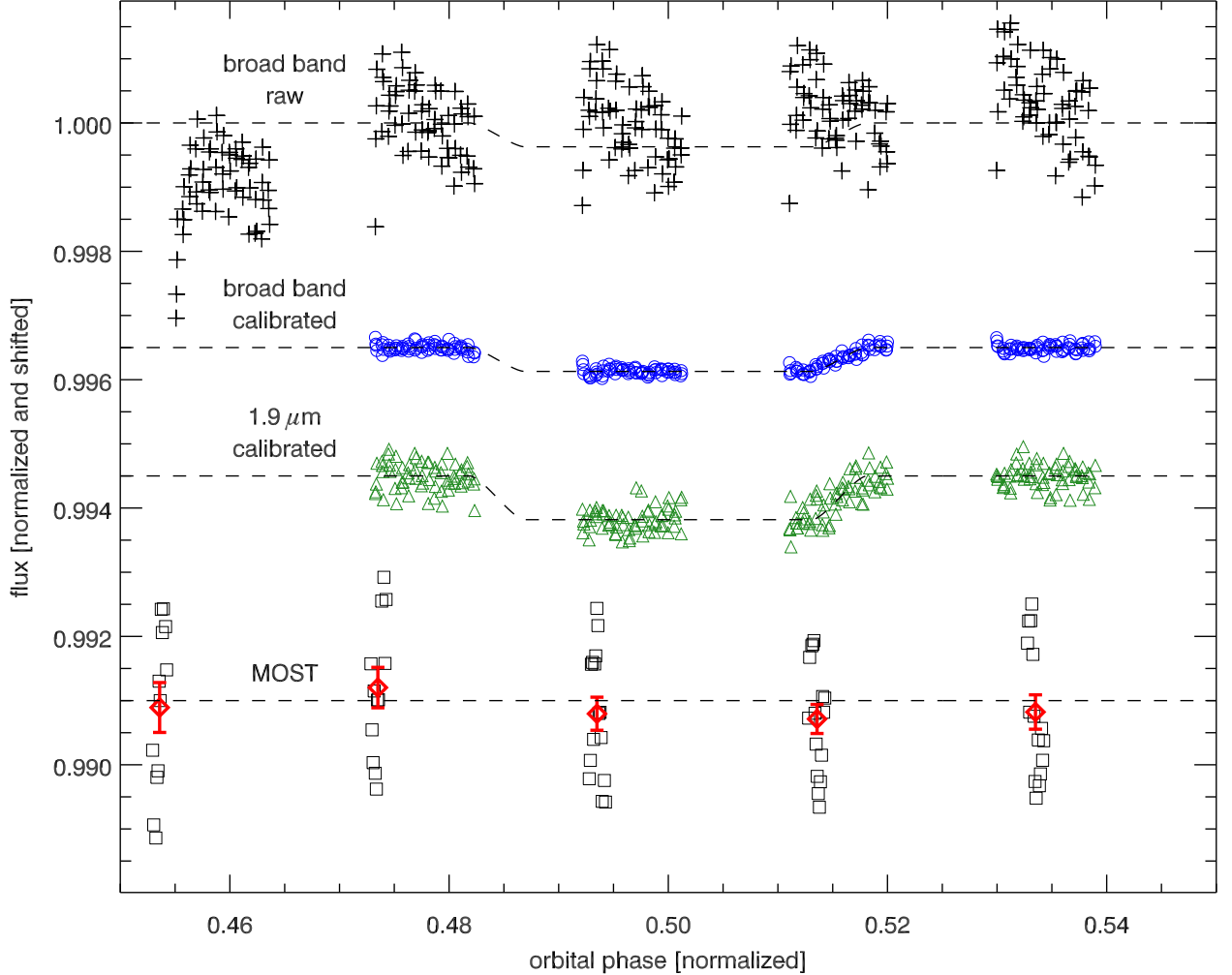


Fig. 1.— This figure shows a set of normalized light curves plotted as a function of orbital phase. Gaps in the data are unavoidable because HD 209458 is not in the continuous viewing zone of Hubble. The top curve is the raw, broad-band, NICMOS data showing large internal scatter and a systematic offset affecting the first orbit. The second curve shows the calibrated, broad-band, NICMOS data (we exclude the first orbit); a shallow eclipse is visible. The third curve shows the calibrated $1.9 \mu\text{m}$ data. The larger eclipse depth at this wavelength (compared to the calibrated broad-band data) is readily apparent. The fourth curve shows the contemporaneous MOST visible photometry data. Both the individual and averaged data are shown. The MOST data are consistent with no changes in the system brightness at visible wavelengths.

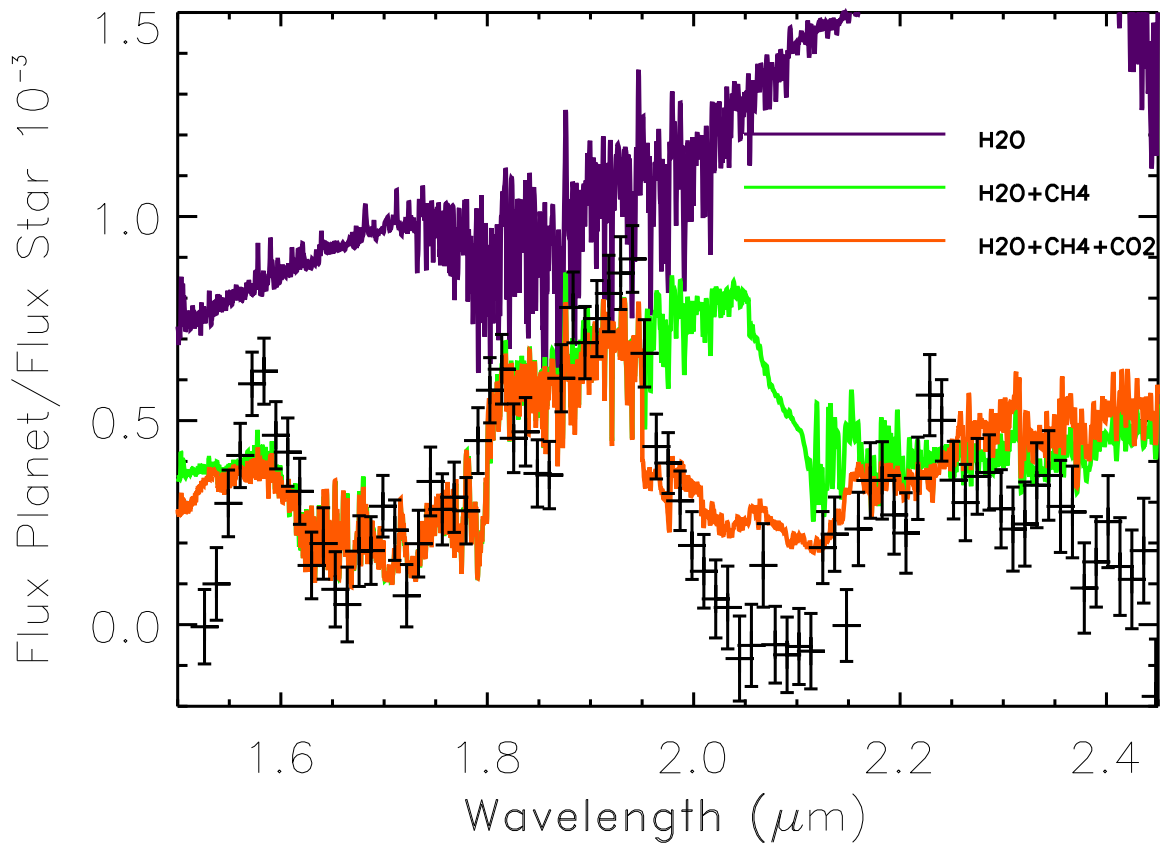


Fig. 2.— A comparison of the observed spectrum (black points with $\pm 1\text{-}\sigma$ error bars) to a sequence of models showing the affect of H_2O , CH_4 , and CO_2 . This comparison shows the portion of the near-infrared spectrum where each molecule makes a significant contribution. CH_4 and H_2O explain most of the spectral features, although additional absorption is needed around $2.0\ \mu\text{m}$ (provided by CO_2). Here, the observed spectrum has been smoothed with a 5-point scrolling boxcar and thus adjacent data points are not statistically independent.

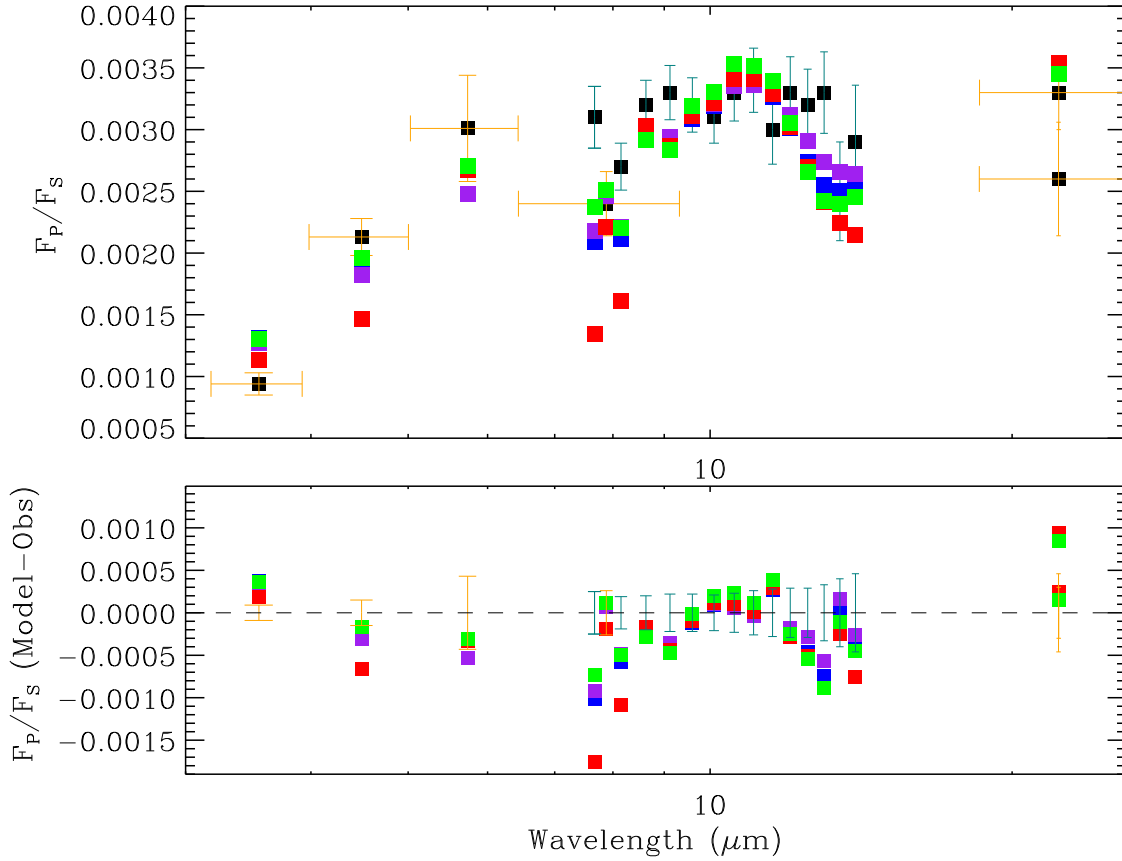


Fig. 3.— Top: Mid-infrared observations compared to synthetic spectra for three models with the tropopause at 0.001 bars (blue), 0.01 bars (purple), & 0.1 bars (green); these models illustrate the range of temperature/composition possibilities consistent with the data. We also show the best fitting model without a temperature inversion (red). Bottom: Model residuals compared to the mid-infrared observations. The model without a tropopause has the largest residuals. The contribution functions and temperature profiles associated with these models are shown in Fig. 5. The mid-infrared photometry are from Knutson et al. 2008 and the mid-infrared spectroscopy are from Swain et al. 2008a.

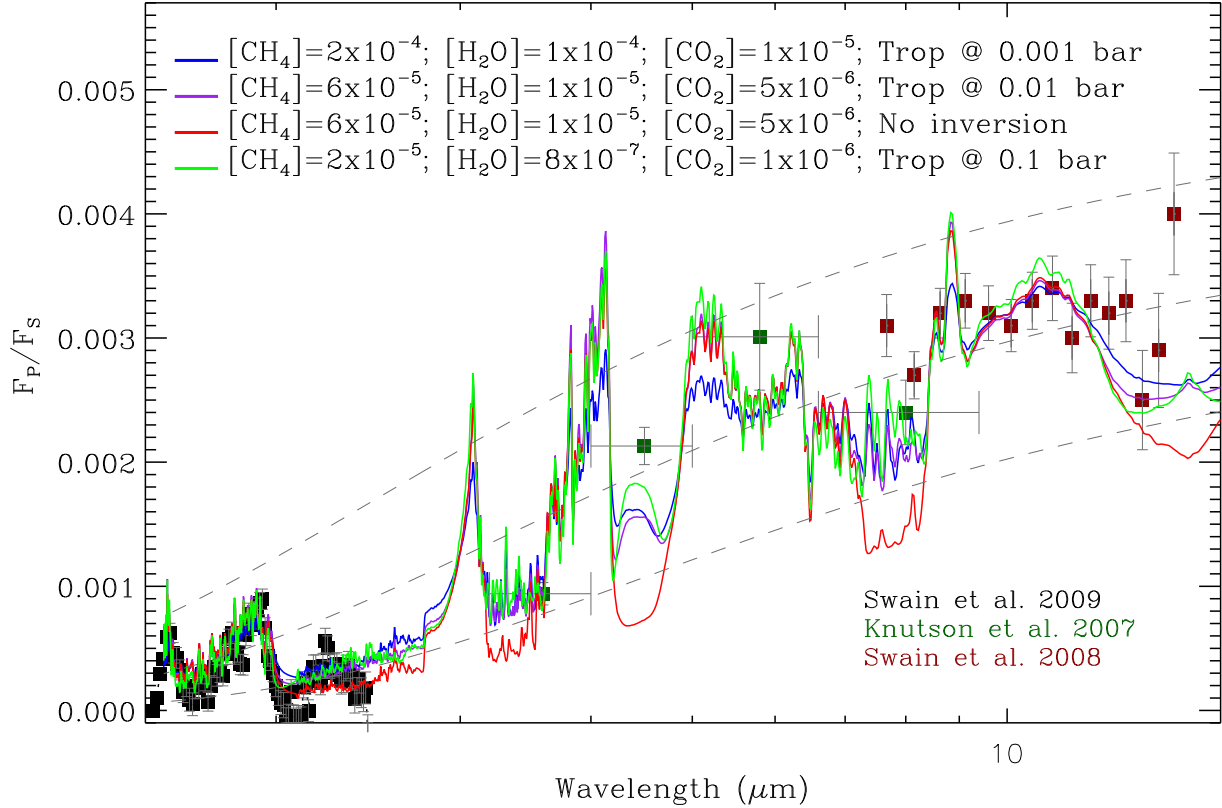


Fig. 4.— The near-infrared and mid-infrared observations compared to synthetic spectra for three models (also shown in Fig. 3) that illustrate the range of temperature/composition possibilities consistent with the data. For each model case, the molecular abundance of CH_4 , H_2O , & CO_2 and the location of the tropopause is given; the contribution functions for each of these models is shown in Fig. 5. The three dashed lines correspond to single-temperature thermal emission models with temperatures of 1400, 1800, and 2200 K; these serve to illustrate how the combination of molecular opacities and the temperature structure cause significant departures from a purely single-temperature thermal emission spectrum. Note that the mid-infrared data are not contemporaneous with the near-infrared data, and attempting to “connect” these data sets with a model spectrum is potentially problematic if significant variability is present.

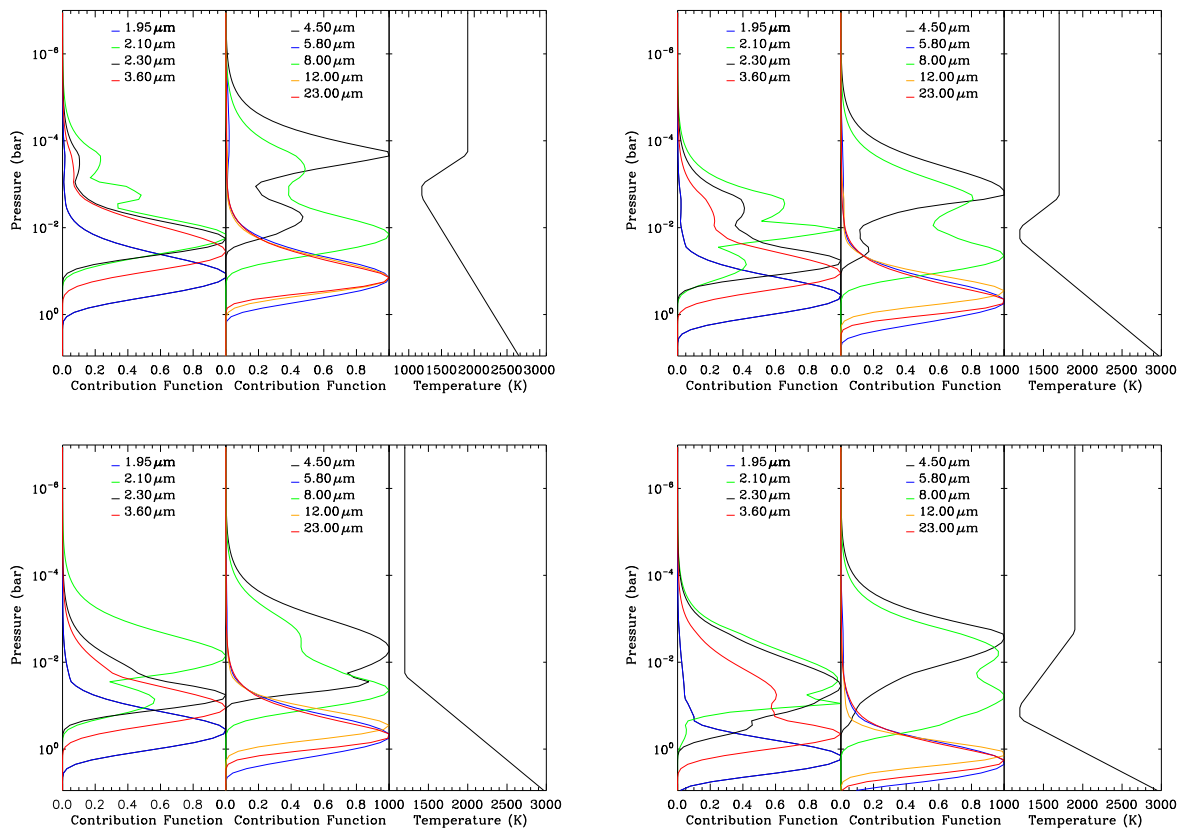


Fig. 5.— The contribution functions for selected wavelengths and the associated temperature profile for each model shown in Figs. 3 & 4; starting from the top left and going clockwise, the models correspond to a tropopause at 0.001 bar, 0.01 bar, 0.1 bar, and no tropopause, respectively. The selected wavelengths correspond to bands of H₂O and CH₄; the contribution function is determined by opacity in each layer, which, in turn, can depend on the local temperature.

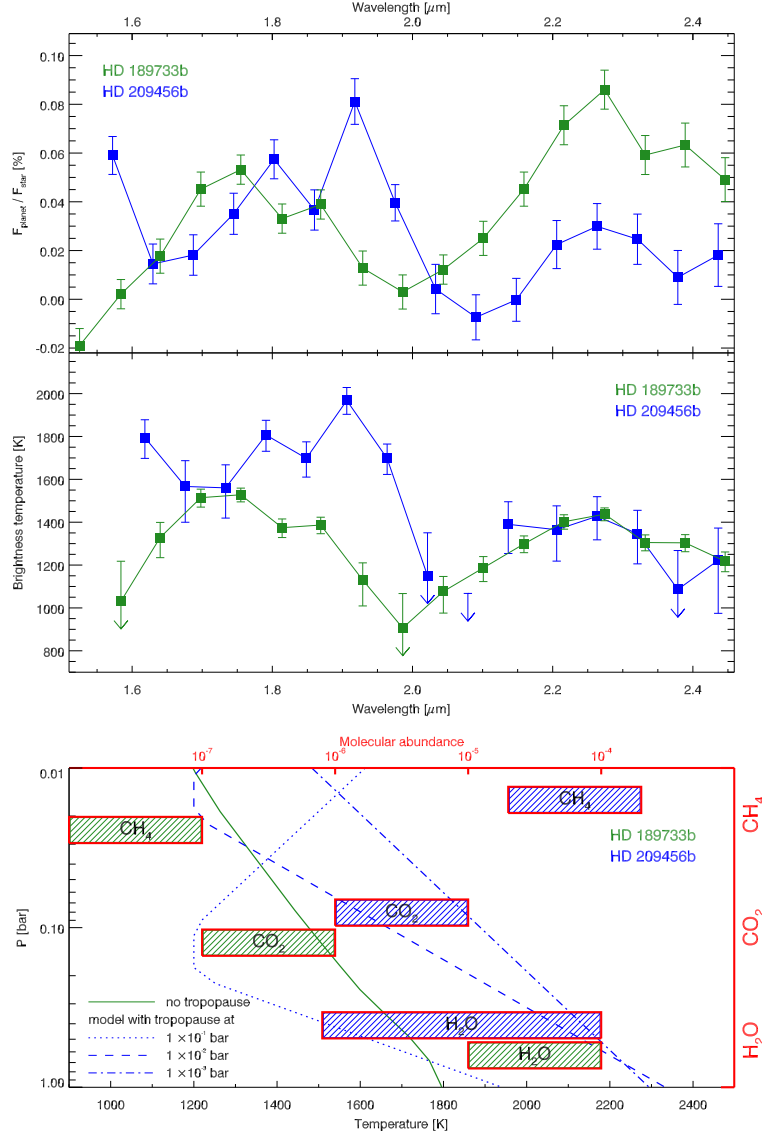


Fig. 6.— Top: The near-infrared dayside emission spectrum of HD 189733b and HD 209458b, showing the significant differences in the observed spectra. Middle: The brightness temperature spectrum of HD 189733b and HD 209458b. The spectra probe similar pressure scales in the dayside atmosphere. The difference in these spectra is due primarily to the presence of (1) significant CH_4 enhancement, and (2) increased temperature in HD 209458b relative to HD 189733b. Bottom: A preliminary comparison of HD 189733b and HD 209458b in terms of the temperature and molecular abundances. The abundance ranges shown here represent the range of solutions we currently identify as consistent with the data. Other temperature/abundance solutions may exist, and thus the results here should be interpreted as indicative. There is a suggestion of enhancement in the abundance of CH_4 and H_2O in HD 209458b relative to HD 189733b; this apparent enhancement needs to be confirmed via additional observations and detailed modeling.